Structure and Interaction Site of the Regulatory Domain of Troponin-C When Complexed with the 96−148 Region of Troponin-I†

Ryan T. McKay, Joyce R. Pearlstone, David C. Corson, Stéphane M. Gagné, Lawrence B. Smillie, and Brian D. Sykes*

MRC Group in Protein Structure and Function Department of Biochemistry 474 Medical Sciences Building University of Alberta, Canada T6G 2H7

Received April 21, 1998; Revised Manuscript Received July 6, 1998

ABSTRACT: The structure of the regulatory domain of chicken skeletal troponin-C (residues 1−90) when complexed with the major inhibitory region (residues 96−148) of chicken skeletal troponin-I was determined using multinuclear, multidimensional NMR spectroscopy. This complex represents the first interaction formed between the regulatory domain of troponin-C and troponin-I after calcium binding in the regulation of muscle contraction. The stoichiometry of the complex was determined to be 1:1, with a dissociation constant in the 1−40 μM range. The structure of troponin-C in the complex was calculated from 1039 NMR distance and 111 dihedral angle restraints. When compared to the structure of this domain in the calcium saturated "open" form but in the absence of troponin-I, the bound structure appears to be slightly more "closed". The troponin-I peptide-binding site was found to be in the hydrophobic pocket of calcium saturated troponin-C, using edited/filtered NMR experiments and chemical shift mapping of changes induced in the regulatory domain upon peptide binding. The troponin-I peptide (residues 96−148) was found to bind to the regulatory domain of troponin-C very similarly, but not identically, to a shorter troponin-I peptide (region 115−131) thought to represent the major interaction site of troponin-I for this domain of troponin-C.

Muscle contraction involves a neural signal cascade resulting in an increased cytosolic calcium concentration. Sliding of the thin filaments (containing actin, tropomyosin and the troponin complex) past the thick filaments (mostly composed of myosin) constitutes the actual muscular contraction. The myosin heads on the surface of the thick filaments do the physical work of contraction by utilizing energy from the hydrolysis of ATP. The troponin complex is the critical unit for calcium regulation of contraction and consists of troponin-C (TnC),[1] TnI, and troponin-T. In the complex troponin-T is postulated to anchor the complex to actin/tropomyosin, TnI inhibits the ATPase activity of myosin, and TnC is the calcium-binding protein. Calcium binding to TnC alters its interaction with TnI, which in turn restores the actomyosin ATPase activity.

The X-ray structure of skeletal TnC revealed a dumbbell-shaped molecule with two EF hand calcium-binding sites in each of its two separate domains (*1*, *2*). In the crystal structure, the two domains are connected by a helical linker; however, NMR solution structures have shown the linker to be unstructured and the two domains to be relatively independent of each other (*3*, *4*). C-TnC contains the high affinity calcium/magnesium sites that are occupied under physiological conditions. N-TnC contains the low-affinity calcium-specific sites which respond to the changes in calcium levels during neuronal signaling (*5*−*9*). Presently, there are X-ray structures of N-TnC and whole TnC under different conditions and with several different metal ion replacements (*1*, *2*, *10*−*12*), and NMR structures of apo and Ca^{2+} saturated skeletal N-TnC (*13*), Ca^{2+} saturated skeletal E41A N-TnC (*14*), Ca^{2+} saturated skeletal TnC (*3*), apo and Ca^{2+} saturated cardiac N-TnC (*15*), and Ca^{2+} saturated cardiac TnC (*4*). N-TnC functions similarly to whole TnC when comparing Ca^{2+} binding affinities (*16*) and overall structure, although isolation of the N-terminal domain subtly affects its stability (*17*). The structures of other homologous proteins such as the myosin light chain (*18*−*21*) and calmodulin (*22*−*24*) have also given insight into the structure and function of troponin-C.

These structures are important in exhibiting how the binding of calcium to TnC affects the physical properties of these proteins, and ultimately how calcium regulates the interaction of the thick and thin filaments. At present, no high-resolution 3D structure of the TnC·TnI complex exists, but 3D structural information for the TnC·TnI complex includes small-angle X-ray scattering experiments (*25*, *26*), two NMR structures of small synthetic TnI peptides bound to TnC (*27*, *28*), and a model based on cross-linking data

† This work was supported by the Medical Research Council Group in Protein Structure and Function, a National Science and Engineering Research Council studentship (R.T.M.), and an Alberta Heritage Foundation for Medical Research Studentship (R.T.M.).

* To whom correspondence should be addressed. Phone: (403) 492-5460. Fax: (403) 492-0886. E-mail: brian.sykes@ualberta.ca.

[1] Abbreviations TnC, troponin-C; TnI, troponin-I; C-TnC, C-terminal domain of troponin-C; N-TnC, N-terminal domain of troponin-C; NMR, nuclear magnetic resonance; NAD, the structural unit of N-TnC comprising the N, A, and D helices; BC, the structural unit made up of the B and C helices; TnI_{96-148}, troponin-I peptide corresponding to residues 96−148; NOE, nuclear Overhauser effect; A_{600}, absorbance at 600 nm; CSI, chemical shift index; A/B, the angle between the A and B helices; B/C, angle between the B and C helices; C/D, angle between the C and D helices; A/D, angle between the A and D helices; $\Delta\delta$, total chemical shift change (Hz) for an individual backbone amide group.

S0006-2960(98)00901-5 CCC: $15.00
Published on Web 08/21/1998

(*29*). The experimental X-ray scattering data has been fit with a model which shows an elongated TnC complexed with a helical central region of TnI. The TnI interacts with the hydrophobic pockets of both the C- and N-terminal domains of TnC. Significant portions of TnI (~50 residues) were distributed at the two ends of the structure. The scattering data show that the centers of mass of TnC and TnI are coincident within experimental error but does not distinguish between parallel versus antiparallel orientations of TnC and TnI, or establish the precise interfacial contacts in the complex. The elongated TnC structure contrasts with the more compact structures of the regulatory and essential light chains of myosin bound to a portion of the heavy chain (*19*−*21*). In addition, recent work by Luo et al. (*30*) using resonance energy transfer to determine the distance between probes attached to Cys^{48} and Cys^{133} of TnI when complexed to TnC found a much shorter distance (41 Å) than would have been expected from the scattering model (70 Å).

The exact regions of TnI that contact TnC in the complex are beginning to be elucidated. Recent studies have shown that TnC and TnI bind in an antiparallel fashion (*5*, *31*−*33*). In this model, C-TnC interacts with the N-domain of TnI, and N-TnC makes calcium-sensitive contacts with both the inhibitory domain (residues 96−116) (*34*) and C-domain (residues 117−182) (*35*) of TnI. C-TnC and N-TnC have been found to bind to adjacent segments of TnI (*36*−*38*). McKay et al. have measured the stoichiometry, affinity, and kinetics of the interaction of N-TnC with residues 115−131 of TnI, and have shown that this complex is kinetically competent to be on the mechanistic pathway for muscle contraction (*39*).

Other regions of troponin-C also contribute to regulation of contraction. The central helix of TnC appears to be important in the formation of the biologically active TnC·TnI complex (*40*, *41*). Recently, C-TnC has been shown to competitively bind residues 1−40 and 104−115 of TnI and also troponin-T (*5*, *29*, *36*−*38*, *42*). Preliminary structures of the C-terminal domain of cardiac and skeletal TnC while bound to the N-terminal domain of cardiac and skeletal TnI, respectively, have been presented (*43*, *44*). These combined data suggest that C-TnC might play a more active role in the release of ATPase inhibition.

An important question to address is the structure of N-TnC in complex with TnI. NMR (*3*, *13*) and X-ray (*10*) structures of N-TnC in the apo and calcium-saturated states revealed large changes in interhelical angles between the NAD and BC structural units upon calcium binding (e.g., ~40° for the A/B angle and ~60° for the C/D angle) which result in the exposure of the hydrophobic pocket. A recent X-ray structure (*11*) confirms that global changes in structure occur although the extent of the change is now under scrutiny (see ref *45* and references therein for review). The hydrophobic pocket has been shown to bind the TnI peptide fragment corresponding to regions 115−131 (*36*, *38*, *39*). It is not known whether this domain opens further in the presence of TnI, or closes around the TnI in some fashion. The structure would be of general interest for other proteins as well, such as calmodulin and the myosin light chains in which homologous domains have been shown to bind helical peptides in a variety of states including closed, semiopen, and open (*18*). Surprisingly, the structure of the highly homologous N-domain of cardiac TnC is closed in the calcium-bound form (*4*, *15*). The determination of the TnC·TnI complex structure is necessary to fully elucidate the mechanism of regulation.

The focus of this work was to determine the structure of skeletal chicken N-TnC in the presence of calcium when bound to skeletal chicken (S96N mutation) TnI_{96-148} and to explore the interaction(s) between the two proteins. It has been shown that the TnI_{96-148} fragment is highly soluble, binds tightly to N-TnC, and retains the full, regulated inhibitory activity of intact TnI (*37*, *38*). Comparisons of the affinities of several TnI peptides for calcium-saturated, intact TnC or N-TnC indicate that residues within the 96−116 and 117−148 regions are primarily responsible for binding to C-TnC and N-TnC, respectively (*36*, *38*). In this study, we have determined the NMR solution structure of N-TnC while bound with TnI_{96-148}, examined the change in N-TnC structure upon peptide binding, and compared the binding of this fragment with that of the shorter TnI peptide corresponding to region 115−131 (*39*). The location of the peptide-binding site on N-TnC was also resolved by monitoring the change in chemical shift of the backbone N-TnC atoms and by utilizing specifically designed NMR experiments to isolate contacts between the protein and peptide.

EXPERIMENTAL PROCEDURES

Proteins. The cloning, expression, and purification of N-TnC was performed as described previously (*46*), and TnI_{96-148} was prepared as described by Pearlstone et al. (*38*). Deuterated N-TnC samples were prepared in the same manner as nondeuterated samples except for preconditioning of expressing cells for growth in M9 limited media containing 80% D_2O (Cambridge Isotopes Inc.) and 20% v/v H_2O. Cell conditioning involved growing transformed cells at 36 °C to a high A_{600} on enriched media. These cells were used to inoculate similar media containing 45% D_2O and grown to an approximate A_{600} of 1, then subsequently used to inoculate 80% D_2O media, and again grown to an A_{600} of 1. Cells were then suspended in 30% v/v glycerol, stored frozen at −80 °C, and/or used to inoculate media of higher D_2O concentrations. Deuteration levels of 88% for N-TnC were determined by mass spectrometry assuming 98% uniform ^{13}C and ^{15}N labeling. The composition and concentration was confirmed by amino acid analysis in triplicate. Protein purity was confirmed by analytical HPLC and SDS−PAGE (*47*).

NMR Sample Preparation. NMR samples (500 μL) used for structure determination consisted of 0.7 mM N-TnC uniformly labeled with ^{15}N, ^{15}N and ^{13}C, or ^{15}N and ^{2}H (88%), 0.9 mM unlabeled TnI_{96-148}, 90% H_2O, 10% D_2O, pH of 6.8 (uncorrected for the deuterium isotope effect), 0.1 mM 2,2-dimethyl-2-silapentane-5-sulfonate as an internal standard, 100 mM KCl, 10 mM imidazole, and 2.8 mM $CaCl_2$.

NMR Experiments. The titration of ^{15}N-labeled N-TnC upon successive 0.3 molar equivalent additions of unlabeled TnI_{96-148} to a final ratio of 1.5:1 TnI_{96-148} to N-TnC was followed using 2D ^{1}H,^{15}N-HMQC NMR spectroscopy at 30 °C. Resonance frequency assignments of ^{1}H, ^{13}C, and ^{15}N, and NOE interproton distance restraints for N-TnC were determined using 2D and 3D NMR experiments as described in Table 1. Experiments were conducted on a Varian Unity-

Table 1: NMR Spectra Acquired and Experimental Conditions Used to Obtain Assignments and NOE Restraints

exp name	nuclei[a]	nt[b]	*x*-pts[c]	*y*-pts	*z*-pts	*x*-sw	*y*-sw	*z*-sw	mix[d]	ref
^{15}N-HMQC	^{1}H,^{15}N	96	1024	128		8000	3000			*72*
^{15}N-HSQC	^{1}H,^{15}N	32	512	256		8000	1647			*58, 73*
TOCSY-hmqc	^{1}H,^{1}H,^{15}N	16	512	128	32	8000	8000	1800	75	*74*
HCCH-TOCSY	^{1}H,^{1}H,^{13}C	32	512	136	32	8000	4000	3165		*75*
CBCA(CO)NNH	^{1}H,^{13}C,^{15}N	40	512	50	30	8000	9174	1650		*58*
^{15}N-noesyhmqc	^{1}H,^{1}H,^{15}N	16	512	118	32	8000	8000	1800	150	*76*
^{15}N-noesyhsqc[e]	^{1}H,^{1}H,^{15}N	20	512	108	32	8000	3003	1650	175	*77*
^{15}N-noesyhsqc	^{1}H,^{1}H,^{15}N	24	512	128	32	8000	7000	1650	70	*77*
^{13}C,^{15}N-noesy[f]	^{1}H,^{1}H,^{13}C/^{15}N	32	704	128	32	8000	7000	3164	150	*78*
HNCO	^{1}H,^{13}C(O),^{15}N	24	512	48	32	8000	1800	1650		*58*
HNCA	^{1}H,^{13}C,^{15}N	32	512	46	32	8000	3922	1650		*79*
HCACO	^{1}H,^{13}C,^{13}C(O)	64	256	30	48	3000	4566	1818		*80*
filter/edit noesy[g]	^{1}H(^{12}C,^{14}N),^{1}H,^{13}C	32	512	96	24	8000	7000	3164	200	*78*
edit/filter noesy	^{1}H,^{1}H(^{12}C,^{14}N),^{13}C	32	512	84	26	8000	5000	3000	110	*81*

[a] The nucleus acquired in each dimension (e.g. ^{1}H,^{15}N indicates proton *x*, nitrogen *y*). [b] The number of transients acquired for each FID. [c] *x*,*y*,*z*-pts and sw is the number of complex points and sweep width in each respective dimension (*x* is the directly detected dimension). [d] Mixing times are given in milliseconds. [e] Executed on an 88% deuterated, uniformly ^{15}N-labeled N-TnC sample. [f] ^{13}C,^{15}N-noesy or "Mother Noesy" is a simultaneously acquired ^{13}C, and ^{15}N-edited-noesy. [g] See Results for details on the filter/edit and edit/filter noesy experiments.

600 except for the edit/filter noesy experiment which was acquired on a Varian Inova 500 NMR spectrometer. All experiments were processed using the software package NMRPipe (*48*) and analyzed using the program PIPP (*49*). Linear prediction was used to increase the number of points in the indirectly detected dimensions by up to half the number of acquired points. Directly and indirectly detected data were then zero filled to twice the number of acquired plus predicted points. Spectra were apodized using a shifted sine bell before Fourier transformation.

Intramolecular NOE Filtering. A sample containing [U-^{13}C]alanine, [^{12}C]valine, and 2-[^{13}C]serine was used to test the filtering efficiency of the intermolecular NOE experiments. The efficiency was determined by the relative suppression of the [^{13}C]alanine and [^{12}C]valine NOE peaks compared to the intramolecular β-^{13}C to α-^{12}C serine cross-peak. The delay periods for the 2 purge pulses were set for proton-carbon coupling constants of 125 and 140 Hz, to give a broader range of filtering efficiency.

NOE Distance Restraints. Only the NOE contacts with the highest assignment confidence were utilized in the structural calculations. This resulted in many observed, ambiguous NOE contacts being abandoned. More ambiguity exists in the spectrum of the N-TnC·TnI_{96-148} complex than for isolated N-TnC because of unassigned NOE cross-peaks from TnI_{96-148}. Peptide resonances were observed to be broad and overlapping. NOE intensities were not classified into calibrated distance restraints due to spin diffusion. A distance restraint of 1.8 to 5 Å was used in the structure calculations for all assigned NOE contacts except for the upper bound of methyl or pseudoatom methylene groups which was extended by 1 Å.

Dihedral Angle Restraints. All nonglycine residues (N-TnC region 4−87) were given a ϕ restraint of $-90 \pm 90°$ unless the CSI (*50*−*52*) values, and $d_{NHH\alpha}(i,i-3)$ NOEs (*53*) indicated a definable secondary structure. For regions of α-helical structure determined by the CSI and NOE measurements, the ϕ angle was restricted during calculations to $-50 \pm 40°$. For β-sheet regions, the ϕ restraint was set to $-120 \pm 40°$.

The ψ-angle restraints were based on the ratio between the backbone amide to intraresidue H_α NOE and the backbone amide to interresidue H_α NOE (*46*). If the intensity of the intraresidue-amide to H_α contact was greater than the amide to the preceding $H_{\alpha(i-1)}$ (ratio of ≥ 1.1) then the secondary structure was considered to be helical and the ψ angle was restricted to $-30 \pm 100°$. On the other hand, if the ratio was less than 0.9, then the ψ was restricted to $-120 \pm 100°$. Ratios between 1.1 and 0.9 were considered indeterminable and no ψ restriction was imposed.

Structure Calculations. Thirty structures of N-TnC were generated with the simulated annealing protocol in XPLOR (*54*), using 18 000 high-temperature steps (90 ps) and 9000 cooling steps (45 ps). The solution structure of calcium-saturated N-TnC (*13*) was used as a starting structure since TnI was expected to bind the open TnC conformation. The calculated structures represent N-TnC while bound to TnI_{96-148}, but no structural NMR data was included for the peptide.

RESULTS

In this paper, we have studied the interaction of the regulatory calcium-binding domain of troponin-C with the major inhibitory region of troponin-I using a variety of 2D/3D multinuclear NMR experiments. N-TnC was uniformly labeled with ^{15}N or ^{15}N/^{13}C whereas the TnI_{96-148} was unlabeled. This allowed for the selection of NMR information pertaining to N-TnC in the complex so that we could determine its structure and any resulting changes induced by the binding of the peptide. Initially, N-TnC was titrated with TnI_{96-148} and the chemical shift changes of N-TnC ^{15}N-HMQC cross-peaks were monitored during the titration (Figure 1). A 1:1 stoichiometry of binding was determined with a dissociation constant on the order of 1−40 μM (data not shown). The spectra in Figure 1 indicate intermediate-fast exchange on the NMR time scale as expected for a K_d in the reported range (*39*). Exchange broadening of cross-peaks made following chemical shifts difficult in a few cases (e.g., Phe[26]). The protein·peptide complex was found to precipitate above a concentration of 0.7 mM as determined by amino acid analysis of the pellet and supernatant. The complex was less soluble in water below a pH of 6.5 and, interestingly, was much less soluble in D_2O. Similar solubility limits in D_2O for intact TnC and TnI have been observed by Olah et al. (*25*).

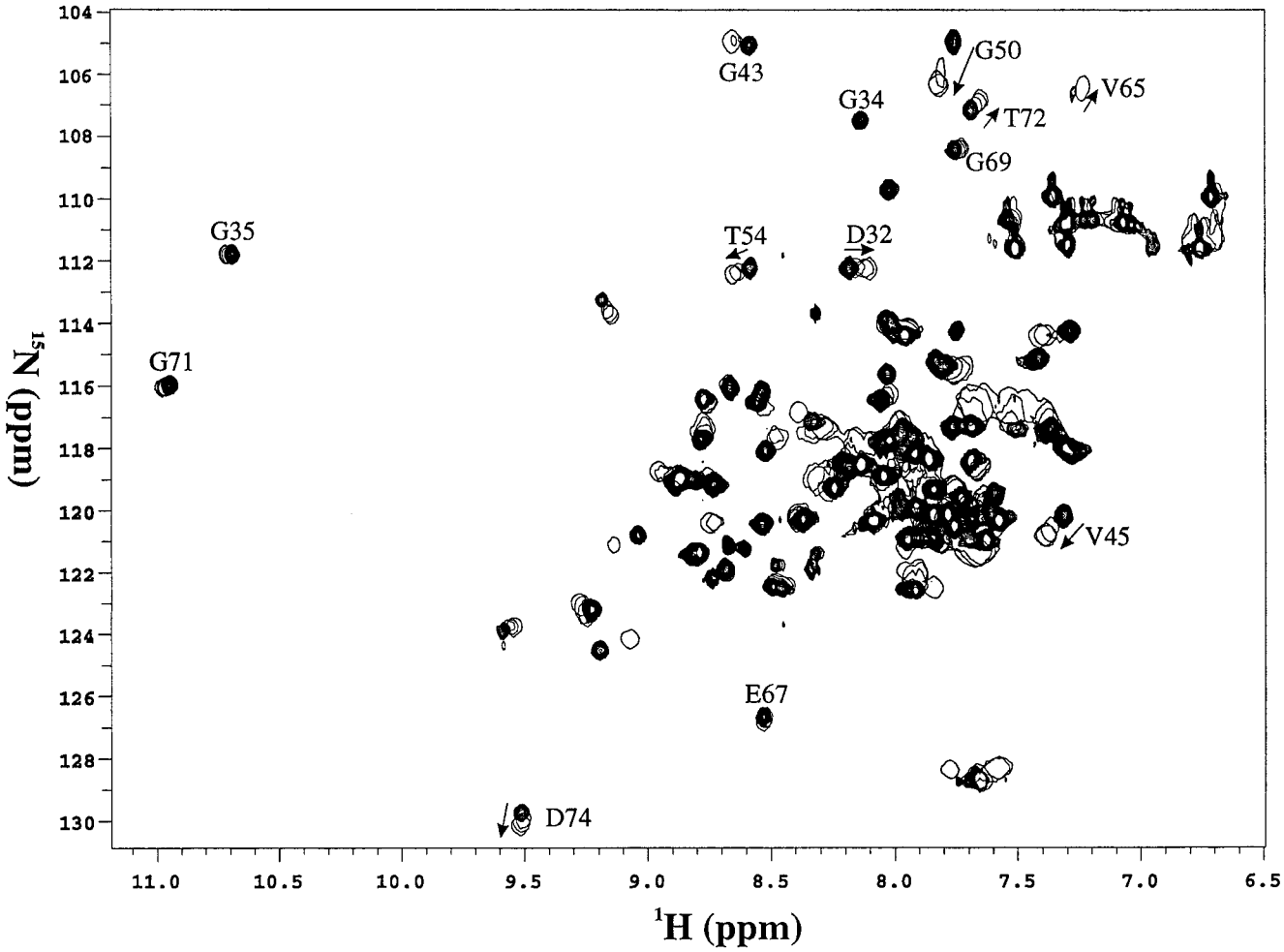

FIGURE 1: Contour plots of the 2D ^{1}H,^{15}N-heteronuclear multiple quantum correlation NMR spectra of N-TnC showing the titration with TnI_{96-148}. The spectra show 0, 0.37, 0.67, and 1 molar equivalents of TnI_{96-148}. Uncomplexed N-TnC cross-peaks are plotted with more contours, while overlaying peaks that appear hollow (single contour) demonstrate the effect of peptide addition during the titration.

Previous binding studies of TnI_{96-148} to troponin-C (*38*) have used fluorescence spectroscopy to follow N-TnC with a single-site (F29W) tryptophan mutation (*55*). Attempts to follow the titration of F29W N-TnC with TnI_{96-148} using NMR under identical sample conditions and concentrations as for the wild-type N-TnC (see Experimental Procedures) were not successful due to insolubility of the F29W N-TnC·TnI_{96-148} complex. Starting concentrations as low as 0.2 mM F29W N-TnC were utilized, but even at these relatively low concentrations, no detectable F29W N-TnC NMR signals remained at a 1:1 ratio of TnI_{96-148} to F29W N-TnC, and no backbone amide chemical shift changes of F29W N-TnC were observed during the titration. The fluorescence spectroscopy binding studies utilizing F29W N-TnC reported no solubility problems in the micromolar concentration range.

One of the major obstacles in determining a protein solution structure using NMR is the molecular weight limit. This limit is dependent, among other things, on how fast the molecule in question undergoes rotational diffusion in solution. The larger the molecule the slower the rotational tumbling, resulting in broadened NMR resonances. A slowly tumbling protein also allows cross-relaxation to occur more rapidly between spins making accurate distance measurements more difficult. The width at half-height of an NMR resonance ($\Delta\nu_{1/2}$) is inversely proportional to the relaxation time (T_2) which characterizes the decay of an NMR signal during multipulse experiments, which is in turn proportional to the rotation time (τ_{Rot}):

$$\Delta\nu_{1/2} = \frac{1}{\pi T_2} \propto \tau_{Rot} \quad (1)$$

We have determined the ^{15}N T_2 for most of the backbone nitrogen nuclei in N-TnC while complexed to TnI_{96-148} (Figure 2A). The average backbone ^{15}N T_2 relaxation time for N-TnC in the complex was 93 ms. Apo N-TnC (*56*) and the highly homologous apo N-domain of cardiac TnC (~10 kDa each) showed average T_2s of 154 and 148 ms, respectively.[2] The expected T_2 for a 16.2 kDa protein at 30 °C is calculated to be 94 ms either by extrapolation from 10 to 16.2 kDa using the average T_2 values of the apo proteins or from standard relaxation theory (*57*). This value agrees well with the observed value. The apparent ^{1}H-NMR line widths of the amide hydrogen nuclei observed for cross-peaks in the HSQC spectra were 28−32 Hz. These are in the expected range for a 16.2 kDa complex by extrapolation from the apparent ~20 Hz line widths observed in HSQC spectra of N-TnC complexed with a smaller TnI peptide

[2] Spyracopoulos, Leo, Gagné, Stéphane, Li, Monica, and Sykes. Dynamics and Energetics of the apo and Ca^{2+}-saturated States of the Regulatory Domain of Cardiac Troponin C. Manuscript in preparation.

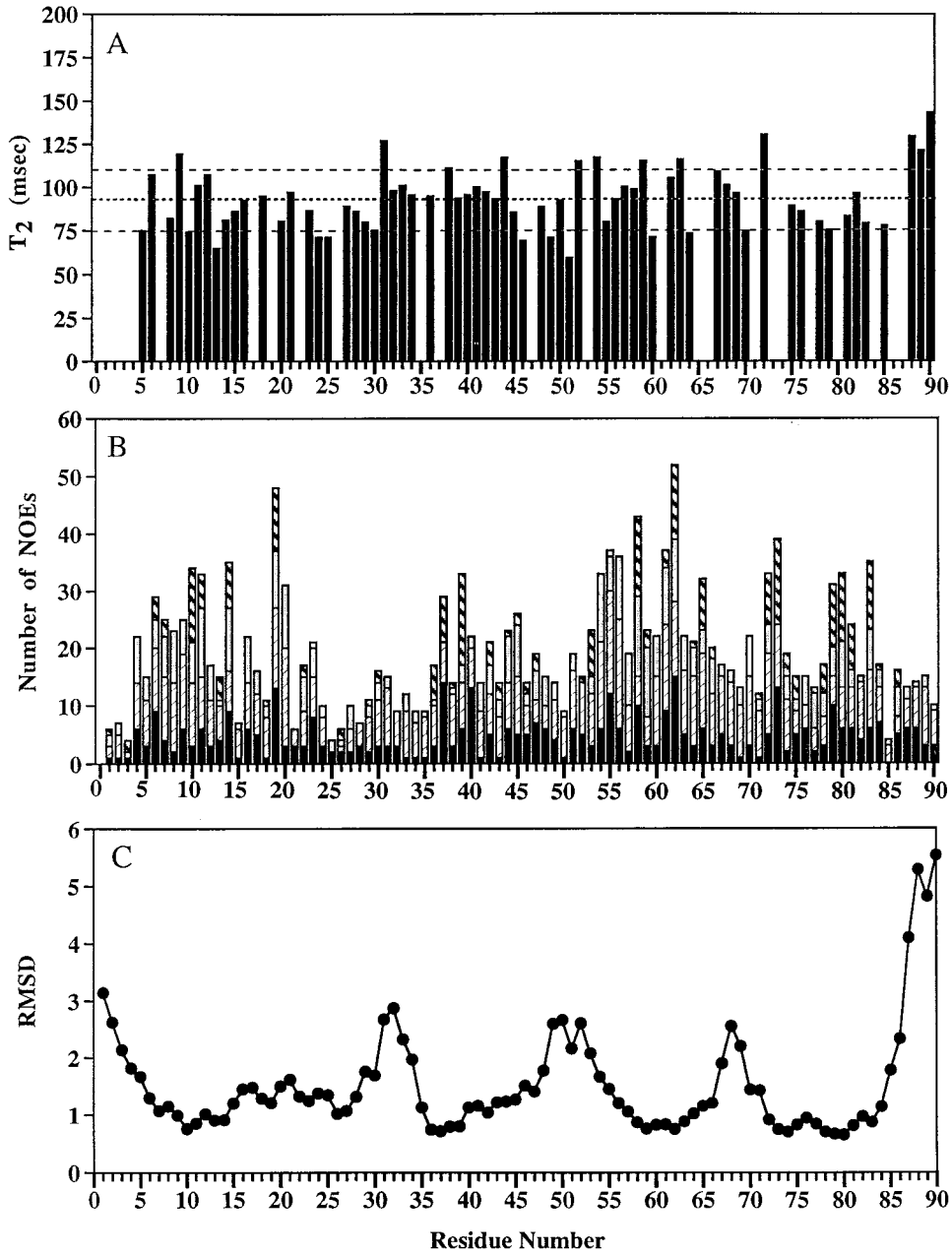

FIGURE 2: (A) Backbone nitrogen T_2 relaxation time (ms) for each of the N-TnC residues subsequently monitored during titration with TnI_{96-148}. The average relaxation time (dotted line) was 93 ms with a standard deviation (dashed lines) of 17 ms. A value of zero for Phe^{26}, and Asp^{66} indicates that the residue could not be followed due to spectral overlap. (B) Distribution of NOEs on a per residue basis used in the structural calculations. Intraresidue, sequential, medium, and long-range contacts are described by solid, dotted crosshatched, shaded, and thick crosshatched columns, respectively. (C) Atomic RMSDs (Å) of backbone atoms (N,C_α,C') for the 30 generated structures. The average RMSD was 1.55 ± 0.35 angstroms for all regions and the RMSD was 1.11 ± 0.25 Å for the well-defined (helices and β-sheet) areas.

(residues 115−131) with a combined molecular weight of ~12 kDa. Thus, the N-TnC·TnI_{96-148} complex appears monomeric in solution. Nonetheless, the effect of the shortened T_2s is propagated exponentially through multi-delay NMR experiments, drastically reducing signal intensity. The loss of NMR signal resulting from the increased signal decay, coupled with limited solubility of the complex, was most noticeable in the HNCACB and HNHA experiments (*58*−*60*).

To help alleviate the spectroscopic problems associated with the large size of the complex, random fractional deuteration of the nonexchangeable protons of N-TnC hydrogen atoms (up to levels of 88%) was employed to increase signal-to-noise and spectral resolution (*61*, *62*). The resulting molecular weight of $^2H,^{13}C,^{15}N$-protein was 10 898 ± 2. The deuterated amide groups were back-exchanged with hydrogen atoms from the solvent to allow NMR detection of the residues in question. Figure 3, panels A and B, demonstrates the increase in cross-peak intensity of the 2D ^{15}N-HSQC NMR spectra for the approximately 96 backbone and side-chain amide groups of N-TnC upon deuteration. The average signal-to-noise ratio based on peak height increased by a factor of ~1.6 while the line widths of the upfield glycine residues narrowed by an average of 5 Hz. Improvement in resolution is a direct result of the extended T_2 relaxation times of the deuterated molecule (*61*,

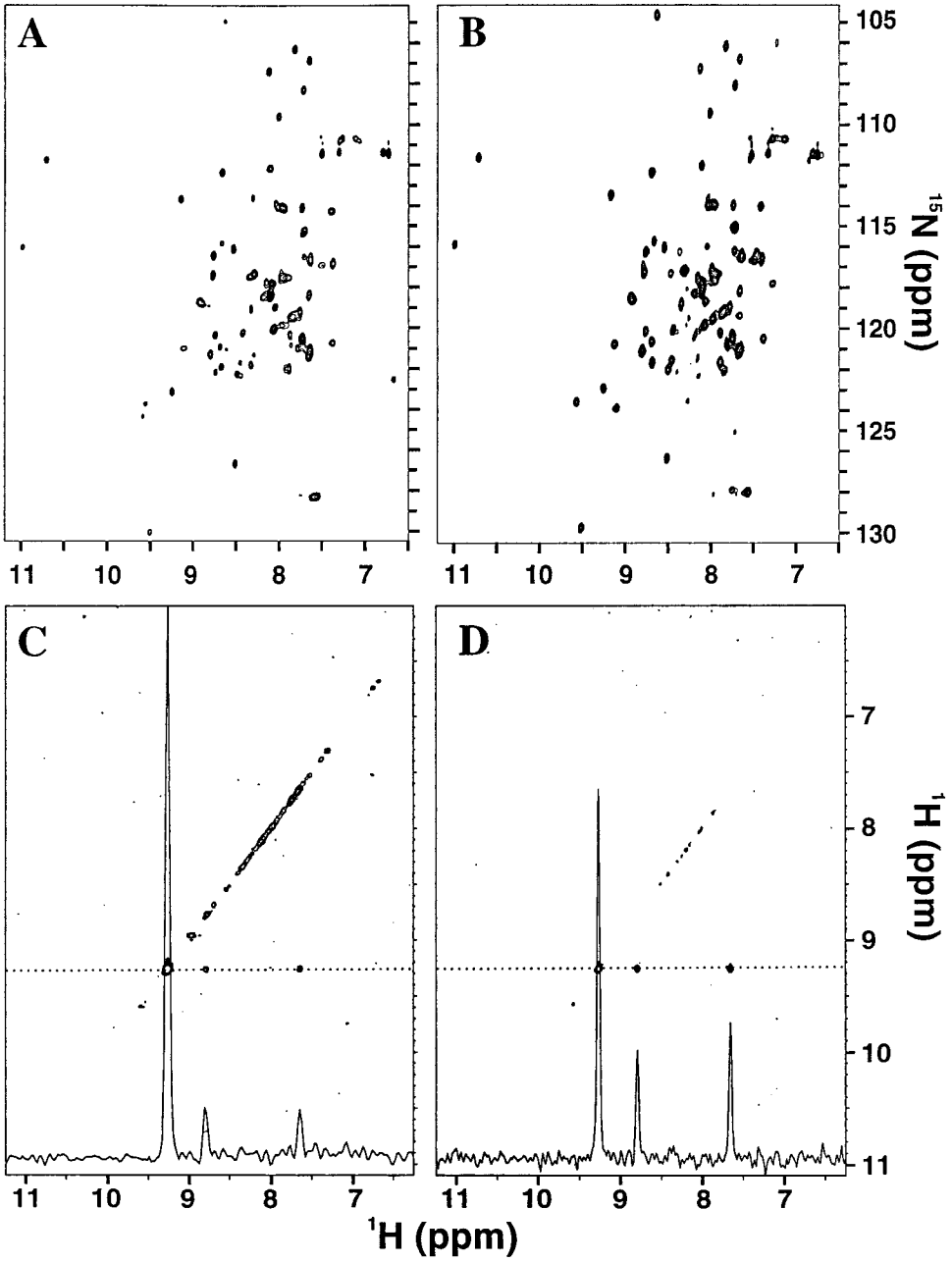

FIGURE 3: Spectra of protonated (A, C), and 88% randomly deuterated (B, D) N-TnC while bound to TnI_{96-148} from (A, B) 2D-^{1}H,^{15}N−HSQC and (C,D) a single ^{15}N spectral plane from a 3D ^{15}N-noesyhsqc. The backbone amide deuterium atoms were back exchanged for hydrogen in the solvent to be visible by NMR in this experiment. In the HSQC spectra, the deuterated sample (B) was on average 1.6 times higher in signal-to-noise than the nondeuterated sample (A). There are several cross-peaks that are too weak to be visible in the protonated sample (e.g., V65 in the upfield portion of the HSQC). The deuterated HSQC was acquired with 8000 Hz (512 t_2 complex points) and 1650 Hz (256 t_1 complex points) sweep widths for hydrogen and nitrogen, respectively, with 64 transients/FID. Only the first 128 t_1 complex points from the spectra of the deuterated sample were processed to make the digital resolution equivalent to the protonated sample. The nondeuterated sample was acquired with a sweep width of 8000 Hz (512 t_2 complex points) and 1800 Hz (128 t_1 complex) for hydrogen and nitrogen respectively with 32 transients per FID. Both experiments were processed using a $\pi/3$ shifted sinebell, zero filled to 1024 t_2 complex points and 512 t_1 complex points, and both samples were approximately 0.7 mM (complex). The difference in the number of transients per acquisition was also compensated in the presentation of the spectra. (C,D) A single plane of the 3D-^{15}N-noesyhsqc experiments with the 1D trace corresponding to Val^{45} (dotted line) shown overlapping in both spectra for ease of comparison is presented. (D) shows an example of the improvement in spectra for sequential assignment that can be obtained by acquiring a narrower (i.e., 3000 Hz for the deuterated sample as compared to the 8000 Hz for the protonated sample) sweep width in the deuterated sample without overlap from upfield aliphatic resonances (see Table 1 for experimental details).

63). Comparison of a single nitrogen plane of the 3D ^{15}N-edited-noesy spectra of deuterated and nondeuterated samples (Figure 3, panels C and D, with 1D trace shown overlaid) clearly shows the improvement in signal-to-noise ratio and resolution. The use of deuterated protein allows the collection of a smaller sweep width and, therefore, improved spectral resolution. The enhanced spectral resolution and signal-to-noise ratio of the deuterated N-TnC in the complex facilitated the identification of more than 90% of all assignable atoms.

Resonance frequencies and interproton NOEs were assigned and analyzed from the 11 NMR experiments shown

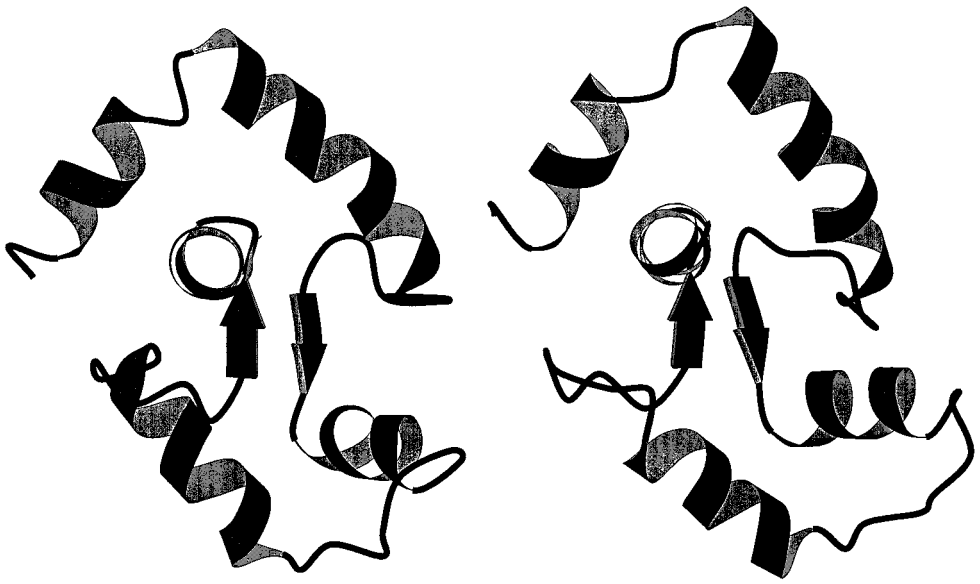

FIGURE 4: Ribbon diagrams showing a comparison of the average, TnI peptide bound, backbone N-TnC structure (left) with that of the calcium-saturated N-TnC structure (right). The diagrams were generated using the program Molscript (*82*).

Table 2: Structural Statistics for N-TnC in Complex with TnI_{96-148}

NOE restraints	
total	1039
intraresidue	411
sequential ($\|i-j\|=1$)	303
medium range ($2 \le \|i-j\| \le 4$)	201
long range ($\|i-j\| \ge 5$)	124
dihedral restraints	
total	111
ϕ	77
ψ	34
RMSD to average structure (Å)	
well-defined regions[a] (N,C_α,C)	1.11 ± 0.25
all regions[b] (N,C_α,C)	1.55 ± 0.35
heavy atoms	2.05 ± 0.31
N-helix (residues 6−14)	0.33 ± 0.08
A-helix (16−29)	0.67 ± 0.28
B-helix (39−47)	0.53 ± 0.20
C-helix (55−65)	0.36 ± 0.14
D-helix (76−86)	0.61 ± 0.23
β-sheet (36−38, 72−74)	0.35 ± 0.14
energies[c] (kcal mol^{-1})	
E_{total}	81 ± 18
E_{NOE}	8 ± 5
$E_{Dihedral}$	6 ± 4
ϕ,ψ in core or allowed regions	95%

[a] N-D helices, and β-sheet. [b] Residues 4−87. [c] The three highest energy structures were removed from the ensemble of 30 structures.

in Table 1 using protocols described previously (ref *64* and references therein). The total numbers of assigned short, medium, and long-range NOEs are given in Figure 2B. Utilizing the program XPLOR (*54*), a total of 30 structures were generated using 1039 NOE and 111 dihedral angle restraints. The structural statistics are presented in Table 2. The N, A, B, C, and D helices and the β-sheet (residues 6−14, 16−29, 39−47, 55−65, 76−86, and 36−38/72−74, respectively) are similar in sequence location and structure to those reported by Gagné et al. (*46*). In the bound structure, the N- and C-terminal residues, as well as the linker regions, are less well-defined. The backbone RMSD for all 30 structures is shown in Figure 2C with an average RMSD of 1.55 ± 0.35 Å. The average RMSD includes all regions of the structure. If the well-defined regions (helices and β-sheet) are superimposed, then the RMSD is 1.11 ± 0.25 Å. The structures were evaluated with the program PROCHECK (*65*), and showed 75% of the backbone dihedral ϕ and ψ angles (30 structures) in the most favored regions with another 21% in the additionally allowed regions. The average structure had 76% of the backbone dihedral angles in the most favored region and 22% in additionally allowed regions. The RMSDs and PROCHECK results indicate that the structure is of medium resolution, and therefore only backbone changes will be evaluated.

Figure 4 shows the ribbon diagram of the average N-TnC structure bound to TnI_{96-148} and the unbound calcium-saturated N-TnC structure (*13*) for comparison. The interhelical angles (residues 6−13, 16−28, 42−48, 55−64, and 75−85 were used for helices N, A, B, C, and D, respectively) for N-TnC bound to TnI_{96-148} are A/B, $92° \pm 11$; B/C, $116° \pm 12$; C/D, $88° \pm 6$; and A/D, $114° \pm 6$. Interestingly, the B−C linker (residues 48−54) appears to be slightly more closed than the NMR and X-ray calcium bound N-TnC structures (*10*, *11*, *13*).[3] Comparison of the average calcium saturated and peptide-bound N-TnC structures show an alteration in the C/D angle, which changes from $68 \pm 5°$ without peptide to $88 \pm 6°$ when bound. This indicates a slight closing of the hydrophobic pocket upon binding.[4,5] The other interhelical angles (e.g., A/B) remain relatively unchanged upon peptide binding within experimental error but do appear to more closely resemble the recent X-ray structures. A recent review has examined the interhelical angles of the X-ray and NMR structures of troponin-C and has addressed the structural and energetic implications of the reported differences (*45*).

In addition to determining the N-TnC structure in the complex, the location of interaction between N-TnC and the

[3] Proper comparison of interhelical angles requires that helix definitions are consistent, and that the same program is used for calculations. Coordinates and definitions were not available from Houdusse et al. (1997) at the time of writing this paper.

[4] An angle of 180° would indicate two helices lying antiparallel with respect to one another.

[5] The PDB file has been assigned the Brookhaven Protein Data Bank accession no. 1BLQ.

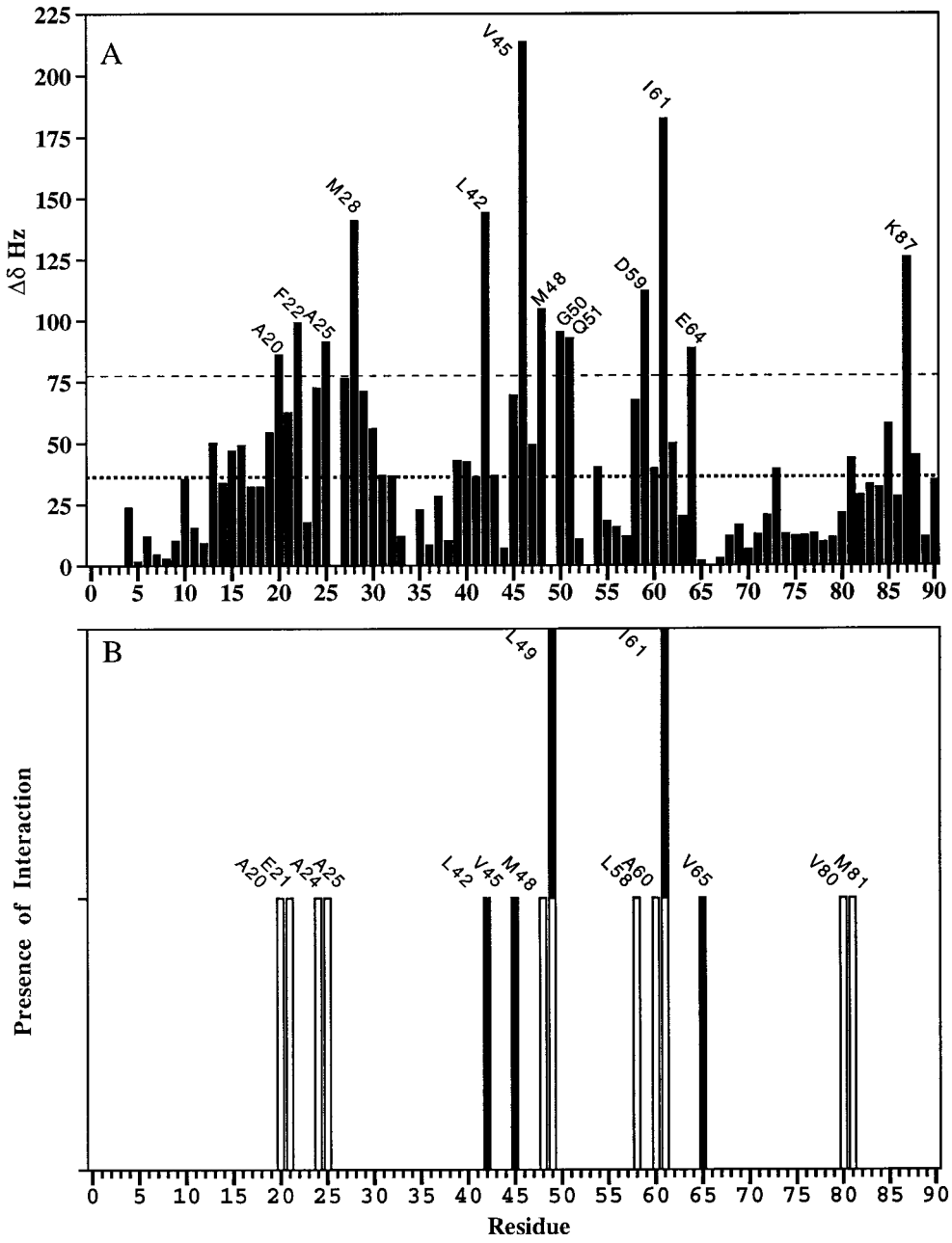

FIGURE 5: (A) The change in chemical shift ($\Delta\delta$) for each backbone amide pair in N-TnC upon binding of TnI_{96-148}. The thin dashed line indicates one standard deviation (41 Hz) above the average (thick dotted line, 39 Hz) $\Delta\delta$. Residues Ala^{20}, Phe^{22}, Ala^{25}, Met^{28}, Leu^{42}, Val^{45}, Met^{48}, Gly^{50}, Gln^{51}, Asp^{59}, Ile^{61}, Glu^{64}, and Lys^{87} demonstrating statistically different $\Delta\delta$ are labeled. Residues Ala^{1}, Ser^{2}, Met^{3}, Phe^{26}, Gly^{34}, Leu^{49}, and Asp^{66} were not followed due to spectral overlap while residues such as Ala^{24}, Ala^{25}, and Lys^{87} may be underestimated (see text). (B) Intermolecular NOEs between TnI_{96-148} and each residue of N-TnC. Residues Ala^{20}, Glu^{21}, Ala^{24}, Ala^{25}, Leu^{42}, Val^{45}, Met^{48}, Leu^{49}, Leu^{58}, Ala^{60}, Ile^{61}, Val^{65}, Val^{80}, and Met^{81} which have unambiguous contacts to the peptide are labeled. The unshaded columns indicate the Filter/Edit-noesy experiment while the black columns represent the Edit/Filter experiment.

TnI peptide was also investigated. The region of interaction was first identified by analyzing the change in chemical shift (*39*) for each N-TnC backbone amide pair upon the addition of TnI_{96-148}. The $\Delta\delta$ for each of the monitored N-TnC residues is presented in Figure 5A. N-TnC backbone amide pairs showing chemical shift changes upon peptide addition greater than 1 standard deviation (thin dashed line) above the average $\Delta\delta$ (thick dotted line) are labeled in the figure and are considered to be statistically different. The residues include Ala^{20}, Phe^{22}, Ala^{25}, Met^{28}, Leu^{42}, Val^{45}, Met^{48}, Gly^{50}, Gln^{51}, Asp^{59}, Ile^{61}, Glu^{64}, and Lys^{87} and thus should represent amino acids directly involved with binding the TnI_{96-148} peptide, immediate neighbors, or residues in the structural hinge regions (*66*). These residues are not all inclusive, and represent only those for which we have the strongest confidence based on chemical shift mapping. Some residues in the molecule could not be followed during the entire titration and therefore do not appear (e.g., Phe^{26}, Leu^{49}, and Asp^{66}), while others (e.g., Ala^{24}, Ala^{25}, and Lys^{87}) may have been underestimated (i.e., followed for only part of the titration).

To further investigate the site of interaction and support the chemical shift information, we performed two sets of filter/edit noesy experiments. These experiments select for

intermolecular NOE contacts and, therefore, identify N-TnC hydrogen atoms within 5 Å of TnI_{96-148} peptide hydrogens. The first NOE experiment (filter/edit) involves filtering out magnetization originating on hydrogen atoms attached to ^{13}C, thus selecting for hydrogen atoms on the peptide (i.e., protons attached to ^{14}N and ^{12}C). The surviving magnetization is then passed, via the NOE, to other protons and standard heteronuclear editing procedures are used to detect only hydrogens attached to ^{13}C. The results of this experiment were scrutinized for any contact that could be intramolecular. For example, if a side chain showed few contacts (i.e., β-protons showed contacts but protons further along the side chain showed no interactions) and/or if the assignment of the particular N-TnC atom was in a crowded spectral region (higher ambiguity), then this contact was considered of lower confidence and not considered for presentation in Figure 5B. Most often a cross-peak was eliminated from consideration if it corresponded to an N-TnC methyl group showing contacts in the filtered experiments to a "methyl group" presumably on the peptide whose resonance frequency was degenerate with an N-TnC methyl group less than 5 Å away. In this case, there exists the possibility, that the observed cross-peak might be a leak in the filtering process. Therefore, only NOE cross-peaks with the highest confidence which could only be intermolecular contacts (i.e., no N-TnC neighbors could account for the contact) were assigned. A second NOE experiment (edit/filter) was performed to verify the contacts identified above. The second experiment was similar to the first, but selected magnetization (editing) from protons attached to ^{13}C and then transferred to hydrogen on ^{12}C. An important advantage of this experiment was that ^{13}C was not decoupled during acquisition; therefore, any "leaks" in the pulse sequence filter were more identifiable by their carbon-proton splitting of ~150 Hz. The results of both the filter/edit experiment and the edit/filter experiments are shown in Figure 5B. From these two experiments, residues Ala^{20}, Glu^{21}, Ala^{24}, Ala^{25}, Leu^{42}, Val^{45}, Met^{48}, Leu^{49}, Leu^{58}, Ala^{60}, Ile^{61}, Val^{65}, Val^{80}, and Met^{81} were unambiguously seen to be in close contact to as yet unassigned TnI_{96-148} hydrogen atoms. Residues which showed contacts but were eliminated based on the above-mentioned criteria include Ala^{8}, Glu^{9}, Leu^{14}, Glu^{16}, Glu^{17}, Asp^{36}, Thr^{39}, Met^{46}, Arg^{47}, Glu^{56}, Phe^{75}, Leu^{79}, Val^{83}, Met^{86}, Lys^{87}, and Glu^{88}. These residues are reported to show that the list of highest confidence contacts is by no means all inclusive.

To better illustrate the spatial relation of interacting residues within the 3D structure, residues of N-TnC which are now thought to be involved in binding TnI_{96-148} are highlighted in Figure 6. The N-TnC molecule is shown in green and residues displaying significant $\Delta\delta$ and/or unambiguous NOE contacts are colored in red. From the $\Delta\delta$ values and the two intermolecular selective NOE experiments, we have strong evidence that TnI_{96-148} binds in the hydrophobic pocket (*67*) of N-TnC. These experiments also draw attention to the predominantly hydrophobic nature of the residues responding to the binding of TnI.

DISCUSSION

In this paper, we followed the titration of labeled N-TnC with unlabeled TnI_{96-148} by ^{1}H,^{15}N-HMQC NMR spectroscopy. The TnI_{96-148} fragment was chosen for its high solubility and full inhibitory effect on the actomyosin complex (*37*, *38*). The spectra seen in these experiments were similar to the spectra seen with the shorter TnI (region 115−131) peptide (*39*). The additional residues in the 96−148 TnI peptide compared to 115−131 peptide apparently do not alter the interaction strength of the complex. The dissociation constants reported by Pearlstone et al. (*38*) using a mutant N-TnC (F29W) (*55*) are smaller than we have observed. The difference in the reported K_d values may be due to the F29W mutation and/or different sample concentrations between the fluorescence and NMR experiments.

It is interesting to compare the effects induced in N-TnC upon binding of TnI_{96-148} in this study with those of a smaller peptide $TnI_{115-131}$ presented previously (*39*). The shorter peptide is thought to comprise the N-TnC-binding site (*36*), but it is not known if the two peptides bind in an identical fashion or if the extra residues in the longer peptide also interact with N-TnC. Comparison of the induced chemical shift changes observed for the two peptides shows that similar but not identical changes are caused by the TnI peptides. In Figure 7A, the chemical shift changes induced by TnI_{96-148} are plotted versus those induced by $TnI_{115-131}$. Not all residues fall on the diagonal demonstrating that they have experienced different shifts from the two peptides. The difference in induced $\Delta\delta$ versus sequence position is plotted in Figure 7B. There does not appear to be an isolated region in the sequence responding differently to either peptide. To evaluate whether these differences are real or a reflection of experimental errors, previously published data for $TnI_{115-131}$ at two salt concentrations are plotted in Figure 7C. While the difference shown might still be real, they are much less than when comparing the two different length peptides. This implies that $TnI_{115-131}$ binds similarly at the two different ionic strengths and also provides an approximation of the experimental error. Interestingly Ala^{25} (Figure 7C) which was extrapolated (*39*) in the high salt sample stands out when compared with the second $TnI_{115-131}$ titration (low salt) induced shifts revealing the relatively large experimental error associated with that residue. When comparing the two different length peptides, residues such as Met^{46}, Ile^{61}, and Lys^{87} show larger chemical shift changes upon addition of TnI_{96-148} while Phe^{26}, Thr^{44}, Val^{65}, and Met^{82} respond more to the smaller peptide. The differences in $\Delta\delta$, despite the similar dissociation constants, indicate that the two peptides do not interact in identical ways though both peptides do interact in the same area and with virtually the same residues. The difference is most likely a result of the additional residues in the larger peptide. This may cause a small change in average secondary structure of the terminal-binding peptide residues and/or an entropic barrier to binding of the larger peptide that may be over come with a slightly larger, stable binding region. In any event, the changes are small when compared to the experimental error and digital resolution of the experiments.

A goal of this paper was to determine the 3D NMR solution structure of skeletal N-TnC while bound to TnI_{96-148}. We have presented an NMR solution structure with a backbone RMSD of 1.5 Å for all regions of N-TnC and 1.1 Å for the well-defined regions. The bound and unbound N-TnC structures are similar except for the BC linker (residues 49−54) and the C/D interhelical angle (bound, 88 ± 6°; unbound, 68 ± 5°). The difference results in a slight closing of the BC helices and, therefore, a slight reduction

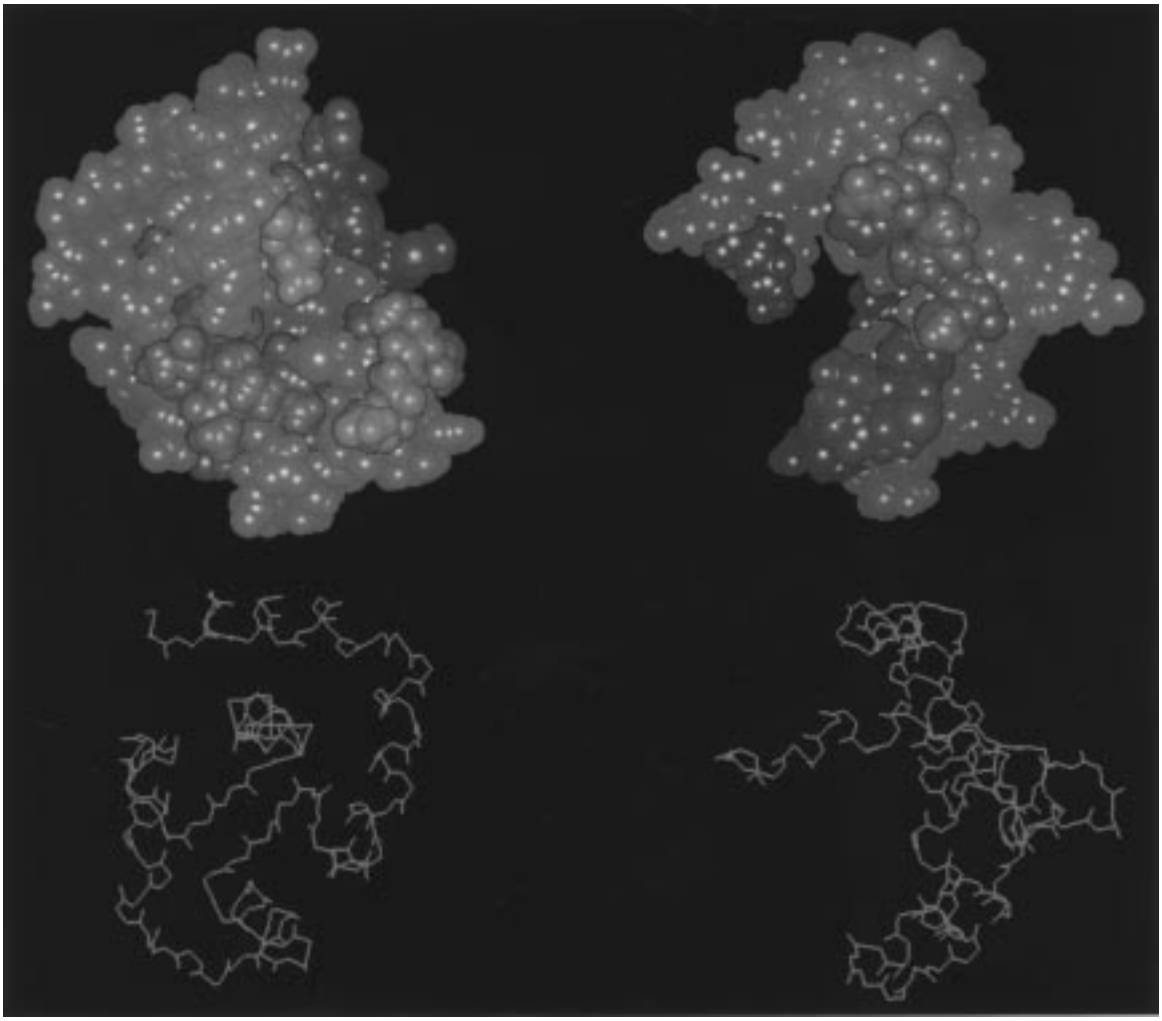

FIGURE 6: Space filling model of N-TnC (green) while bound to TnI_{96-148}. Residues Ala^{20}, Glu^{21}, Phe^{22}, Ala^{24}, Ala^{25}, Met^{28}, Leu^{42}, Val^{45}, Met^{48}, Leu^{49}, Gly^{50}, Gln^{51}, Leu^{58}, Asp^{59}, Ala^{60}, Ile^{61}, Glu^{64}, Val^{65}, Val^{80}, Met^{81}, and Lys^{87} which showed statistically different changes in $\Delta\delta$ and/or intermolecular NOEs are shown in red. The two images are rotated approximately 90° to one another, and the average backbone orientation corresponding to each space filling model was included (bottom) for easier viewer orientation. The binding site is a channel formed by the hydrophobic pocket running laterally across the protein.

in the surface area of the hydrophobic pocket. This suggests that the N-TnC may "clamp" down on the TnI peptide; however, the change is small in comparison to the changes of N-TnC from apo to the calcium-saturated state (*13*). Interestingly the recently reported apo and calcium-saturated cardiac N-TnC (*15*) and calcium-saturated whole cardiac TnC (*4*) structures do not exhibit the expected opening of the hydrophobic pocket. Identifying the exact location of TnI_{96-148} binding has become even more important in light of this new structural information.

Another goal was to identify the location of TnI_{96-148} binding on N-TnC. The combined use of chemical shift mapping which indicates alterations in the local magnetic environment, and the intermolecular NOE experiments which provide direct intermolecular hydrogen contacts within 5 Å, allow an efficient method for identifying which hydrogen atoms are involved in intermolecular van der Waals contact. The binding of TnI_{96-148} presumably disrupts the TnC dimer [~30% dimerized at 1 mM (*13*, *68*)] in solution which may account for some of the difference seen in the unbound versus bound structures. This is especially relevant since dimerization was shown to occur primarily in the N-domain (*3*). We have attempted to select residues experiencing functionally relevant changes by highlighting only those with statistically different shifts (i.e., the selection of one standard deviation above the average). We are therefore attempting to discern between primary effects of binding and secondary effects of small remote changes in the environment.

Our results agree with previously reported cross-linking studies (*33*, *69*, *70*). Mutational work by Pearlstone et al. (*55*, *71*) that identified residues making up the hydrophobic pocket match those residues found in our study which bind to TnI_{96-148}. The present study has not yet identified which TnI_{96-148} residues are involved in binding to N-TnC. However, primary sequence inspection of TnI revealed a common characteristic between TnI regions 108−115 and 137−144 (*5*). Later, a 3-fold repeated sequence (designated α, β, and γ) which is highly conserved among species involving residues ~101−114, ~121−132, and ~135−146 was reported (*38*). In recent reports (*36*, *39*), residues 115−131 were shown to be involved in binding to the hydrophobic patch of N-TnC, and residues 140−148 were identified as playing a crucial role in inhibition of actomyosin S1 ATPase (*37*). Coupled with abundant evidence (summarized in ref *36*) for C-TnC and the central helix interaction with TnI residues 96−115, the present data indicates strongly that the

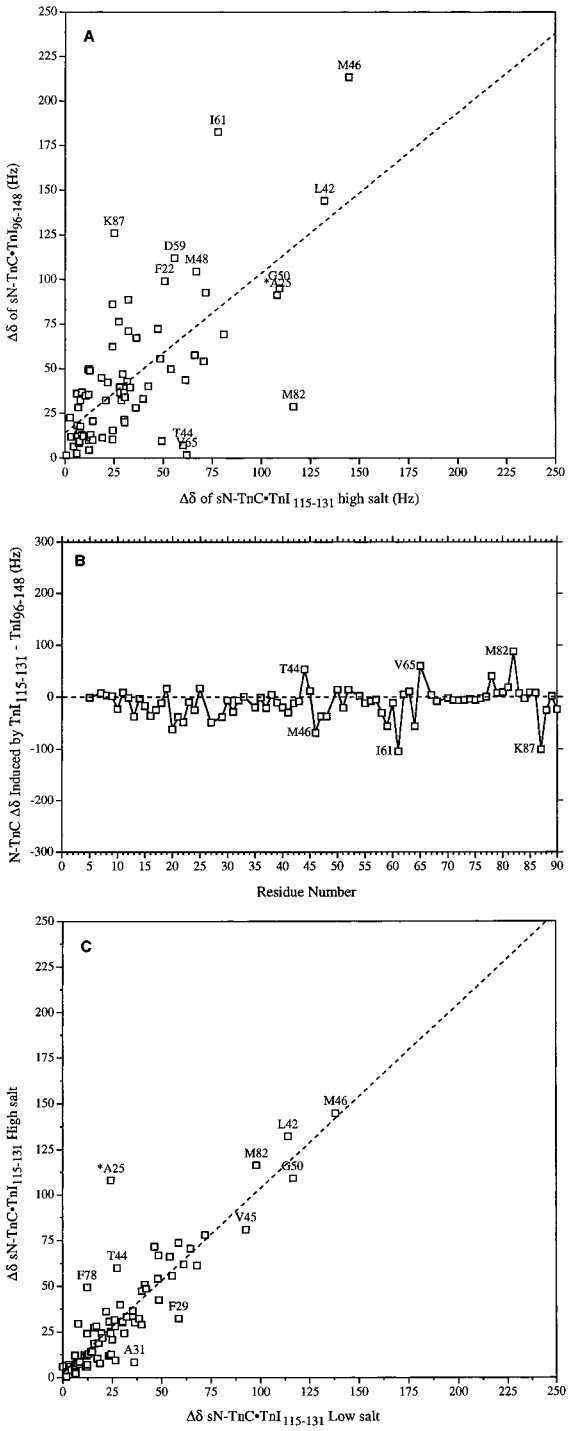

FIGURE 7: Comparison of the change in chemical shift induced in N-TnC residues upon TnI peptide binding. (A) Comparison of TnI_{96-148} (*y*-axis) binding induced N-TnC chemical shift changes when plotted against the changes caused by $TnI_{115-131}$ (*x*-axis) in high salt. The least-squares fit (dashed line) showed a slope of 0.90 and a *y*-intercept of 14. (B) Shows the difference ($\Delta\delta$ induced by $TnI_{115-131}$ − $\Delta\delta$ induced by TnI_{96-148}) in $\Delta\delta$ for each N-TnC residue followed when comparing $TnI_{115-131}$ to TnI_{96-148} binding. (C) The change in chemical shift for N-TnC residues upon binding of $TnI_{115-131}$ in high salt (*y*-axis) plotted versus the change caused by $TnI_{115-131}$ in low salt (*x*-axis) for comparison. A least-squares fit (dashed line) showed a slope of 1.01 and a *y*-intercept of 2.6 implying very similar induced changes.

96−131 region of TnI is intimately involved in binding to the hydrophobic patch regions of both C- and N-TnC.

We have determined the structure of N-TnC while bound to TnI_{96-148} and the site of interaction between N-TnC and TnI_{96-148} using the $\Delta\delta$ and intermolecular NOE experiments. This paper has shown that TnI_{96-148} and N-TnC interact through the calcium regulated hydrophobic pocket of N-TnC. The lack of significant structural changes in N-TnC also indicates that the binding of calcium and the exposure of the hydrophobic pocket is sufficient to prepare N-TnC for interaction with the TnI peptide. Future work will logically lead to determining the structure of the TnI peptide while bound to the N-domain and eventually to the structure of the intact TnC·TnI complex.

ACKNOWLEDGMENT

Thanks to Gerry McQuaid and Bruce Lix for upkeep of the NMR spectrometers, to Lewis E. Kay for NMR pulse sequences, the Protein Engineering Network of Centres of Excellence for use of the Unity 600 NMR spectrometer, Brian Tripet for making his data available before publication and productive discussions. Thanks to Linda Saltibus, Monica Li, Carolyn Slupsky, and Larry Calhoun for advice and help during this work and especially to Leo Spyracopoulos for careful reading of this manuscript and many helpful suggestions.

REFERENCES

1. Herzberg, O., and James, M. N. G. (1988) *J. Mol. Biol. 203*, 761−779.
2. Satyshur, K. A., Rao, S. T., Pyzalska, D., Drendal, W., Greaser, M., and Sundaralingham, M. (1988) *J. Biol. Chem. 263*, 1628−1647.
3. Slupsky, C. M., and Sykes, B. D. (1995) *Biochemistry 34*, 15953−15964.
4. Sia, S. K., Li, M. X., Spyracopoulos, L., Gagné, S. M., Liu, W., Putkey, J. A., and Sykes, B. D. (1997) *J. Biol. Chem. 272*, 18216−18221.
5. Farah, C. S., and Reinach, F. C. (1995) *FASEB J. 9*, 755−767.
6. Li, M. X., Gagné, S. M., Tsuda, S., Kay, C. M., Smillie, L. B., and Sykes, B. D. (1995) *Biochemistry 34*, 8330−8340.
7. Head, J. F., and Perry, S. V. (1974) *Biochem. J. 137*, 145−154.
8. Weeks, R. A., and Perry, S. V. (1978) *Biochem. J. 173*, 449−457.
9. Potter, J. D., and Johnson, J. D. (1982) in *Calcium and Cell Function* (Cheung, W. Y., Ed.) Vol. 2, pp 145−169, Academic Press, Inc., New York.
10. Strynadka, N. C. J., Cherney, M., Sielecki, A. R., Li, M. X., Smillie, L. B., and James, M. N. G. (1997) *J. Mol. Biol. 273*, 238−255.
11. Houdusse, A., Love, M. L., Dominguez, R., Grabarek, Z., and Cohen, C. (1997) *Structure 5*, 1695−1711.
12. Rao, S. T., Satyshur, K. A., Greaser, M. L., and Sundaralingam, M. (1996) *Acta Crystallogr. Sect. D 52*, 916−922.
13. Gagné, S. M., Tsuda, S., Li, M. X., Smillie, L. B., and Sykes, B. D. (1995) *Nat. Struct. Biol. 2*, 784−789.
14. Gagné, S. M., Li, M. X., and Sykes, B. D. (1997) *Biochemistry 36*, 4386-4392.
15. Spyracopoulos, L., Li, M. X., Sia, S. K., Gagné, S. M., Chandra, M., Solaro, R. J., and Sykes, B. D. (1997) *Biochemistry 36*, 12138−12146.
16. Li, M. X., Chandra, M., Pearlstone, J. R., Racher, K. I., Trigo-Gonzalez, G., Borgford, T., Kay, C. M., and Smillie, L. B. (1994) *Biochemistry 33*, 917−925.
17. Fredricksen, S. R., and Swenson, C. A. (1996) *Biochemistry 35*, 14012−14026.
18. Houdusse, A., and Cohen, C. (1995) *Proc. Natl. Acad. Sci. U.S.A. 92*, 10644−10647.

19. Xie, X., Harrison, D. H., Schlichting, I., Sweet, R. M., Kalabokis, V. N., Szent-Gyorgyi, A. G., and Cohen, C. (1994) *Nature 368*, 306−312.
20. Rayment, I., Holden, H. M., Whittaker, M., Yohn, C. B., Lorenz, M., Holmes, K. C., and Milligan, R. A. (1993) *Science 261*, 58−65.
21. Rayment, I., Rypniewski, W. R., Schmidt-Base, K., Smith, R., Tomchick, D. R., Benning, M. M., Winkelmann, D. A., Wesenberg, G., and Holden, H. M. (1993) *Science 261*, 50−58.
22. Babu, Y. S., Bugg, C. E., and Cook, W. J. (1988) *J. Mol. Biol. 204*, 191−204.
23. Kretsinger, R. H., Rudnick, S. E., and Weissman, L. J. (1986) *J. Inorg. Biochem. 28*, 289−302.
24. Ikura, M., Clore, G. M., Gronenborn, A. M., Zhu, G., Klee, C. B., and Bax, A. (1992) *Science 256*, 632−638.
25. Olah, G. A., Rokop, S. E., Wang, C.-L. A., Blechner, S. L., and Trewhella, J. (1994) *Biochemistry 33*, 8233−8239.
26. Olah, G. A., and Trewhella, J. (1994) *Biochemistry 33*, 12800−12806.
27. Campbell, A. P., and Sykes, B. D. (1991) *J. Mol. Biol. 222*, 405−421.
28. Campbell, A. P., Van Eyk, J. E., Hodges, R. S., and Sykes, B. D. (1992) *Biochim. Biophys. Acta 1160*, 35−54.
29. Ngai, S.-M., Sönnichsen, F. D., and Hodges, R. S. (1994) *J. Biol. Chem. 269*, 2165−2172.
30. Luo, Y., Wu, J.-L., Gergely, J., and Tao, T. (1997) *Biochemistry 36*, 11027−11035.
31. Sheng, Z., Pan, B. S., Miller, T. E., and Potter, J. D. (1992) *J. Biol. Chem. 267*, 25407−25413.
32. Krudy, G. A., Kleerekoper, Q., Guo, X., Howarth, J. W., Solaro, R. J., and Rosevear, P. R. (1994) *J. Biol. Chem. 269*, 23731−23735.
33. Kobayashi, T., Grabarek, Z., Gergely, J., and Collins, J. H. (1995) *Biochemistry 34*, 10946−10952.
34. Talbot, J. A., and Hodges, R. S. (1981) *J. Biol. Chem. 256*, 2798−2802.
35. Farah, C. S., Miyamoto, C. A., Ramos, C. H. I., da Silva, A. C. R., Quaggio, R. B., Fujimori, K., Smillie, L. B., and Reinach, F. C. (1994) *J. Biol. Chem. 269*, 5230−5240.
36. Tripet, B. P., Van Eyk, J. E., and Hodges, R. S. (1997) *J. Mol. Biol. 271*, 728−750.
37. Van Eyk, J. E., Thomas, L. T., Tripet, B. P., Wiesner, R. J., Pearlstone, J. R., Farah, C. S., Reinach, F. C., and Hodges, R. S. (1997) *J. Biol. Chem. 272*, 10529−10537.
38. Pearlstone, J. R., Sykes, B. D., and Smillie, L. B. (1997) *Biochemistry 36*, 7601−7606.
39. McKay, R. T., Tripet, B. P., Hodges, R. S., and Sykes, B. D. (1997) *J. Biol. Chem. 272*, 28494−28500.
40. Ramakrishnan, S., and Hitchcock-DeGregori, S. E. (1996) *Biochemistry 35*, 15515−15521.
41. Jha, P. K., Mao, C., and Sarkar, S. (1996) *Biochemistry 35*, 11026−11035.
42. Pearlstone, J. R., and Smillie, L. B. (1995) *Biochemistry 34*, 6932−6940.
43. Gasmi-Seabrook, G., Howarth, J. W., Finley, N., Abbott, M. B., Brito, R. M., and Rosevear, P. R. (1998) *Biophys. J. 74*, A299.
44. Vassylyev, D. G., Takeda, S., Wakatuski, S., Maeda, K., and Maeda, Y. (1998) *Biophys. J. 74*, A53.
45. Gagné, S. M., Li, M. X., McKay, R. T., and Sykes, B. D. (1998) *Biochem. Cell Biol.* (In press).
46. Gagné, S. M., Tsuda, S., Li, M. X., Chandra, M., Smillie, L. B., and Sykes, B. D. (1994) *Protein Sci. 3*, 1961−1974.
47. Zhou, N. E., Kay, C. M., and Hodges, R. S. (1994) *Protein Eng. 7*, 1365−1372.
48. Delaglio, F., Grzesiek, S., Vuister, G. W., Zhu, G., Pfeifer, J., and Bax, A. (1995) *J. Biomol. NMR 6*, 277−293.
49. Garrett, D. S., Powers, R., Gronenborn, A. M., and Clore, G. M. (1991) *J. Magn. Reson. 95*, 214−220.
50. Wishart, D. S., and Sykes, B. D. (1994) *Methods Enzymol. 239*, 363−392.
51. Wishart, D. S., and Sykes, B. D. (1994) *J. Biomol. NMR 4*, 171−180.
52. Wishart, D. S., Sykes, B. D., and Richards, F. M. (1991) *J. Mol. Biol. 222*, 311−333.
53. Wüthrich, K. (1986) *NMR of proteins and nucleic acids*, John Wiley & Sons, New York.
54. Brünger, A. T. (1992) *X-PLOR Version 3.1 A system for X-ray Crystallography and NMR*, Yale University Press, New Haven.
55. Pearlstone, J. R., Borgford, T., Chandra, M., Oikawa, K., Kay, C. M., Herzberg, O., Moult, J., Herklotz, A., Reinach, F. C., and Smillie, L. B. (1992) *Biochemistry 31*, 6545−6553.
56. Gagné, S. M., Tsuda, S., Spyracopoulos, L., Kay, L. E., and Sykes, B. D. (1998) *J. Mol. Biol. 278*, 667−686.
57. Abragam, A. (1961) *Principles of Nuclear Magnetism*. International Series on Monographs on Physics (Adair, R. K., Edwards, S. F., Ehrenreich, H., Llewellyn Smith, C. H., and Rees, M., Eds.) p 32, Oxford University Press, Toronto.
58. Muhandiram, D. R., and Kay, L. E. (1994) *J. Magn. Reson., Ser. B 103*, 203-216.
59. Wittekind, M., and Mueller, L. (1993) *J. Magn. Reson.*, Ser. B *101*, 201−205.
60. Vuister, G. W., and Bax, A. (1993) *J. Am. Chem. Soc. 115*, 7772−7777.
61. LeMaster, D. M. (1990) *Q. Rev. Biophys. 23*, 133−174.
62. Grzesiek, S., Wingfield, P., Stahl, S., Kaufman, J. D., and Bax, A. (1995) *J. Am. Chem. Soc. 117*, 9594−9595.
63. Grzesiek, S., Anglister, J., Ren, H., and Bax, A. (1993) *J. Am. Chem. Soc. 115*, 4369−4370.
64. Slupsky, C. M. (1995) in *Thesis: Biochemistry*, University of Alberta, Edmonton.
65. Laskowski, R. A., MacArthur, M. W., Moss, D. S., and Thorton, J. M. (1993) *J. Appl. Crystallogr. 26*, 283−290.
66. Shuker, S. B., Hajduk, P. J., Meadows, R. P., and Fesik, S. W. (1996) *Science 274*, 1531−1534.
67. Herzberg, O., Moult, J., and James, M. N. G. (1986) *J. Biol. Chem. 261*, 2638−2644.
68. Slupsky, C. M., Kay, C. M., Reinach, F. C., Smillie, L. B., and Sykes, B. D. (1995) *Biochemistry 34*, 7365−7375.
69. Leszyk, J., Grabarek, Z., Gergely, J., and Collins, J. H. (1990) *Biochemistry 29*, 299−304.
70. Kobayashi, T., Leavis, P. C., and Collins, J. H. (1996) *Biochim. Biophys. Acta 1294*, 25−30.
71. Pearlstone, J. R., McCubbin, W. D., Kay, C. M., Sykes, B. D., and Smillie, L. B. (1992) *Biochemistry 31*, 9703−9708.
72. Bax, A., Griffey, R. H., and Hawkins, B. L. (1983) *J. Magn. Reson. 55*, 301−315.
73. Kay, L. E., Keifer, P., and Saarinen, T. (1992) *J. Am. Chem. Soc. 114*, 10663−10665.
74. Marion, D. C., Driscoll, P. C., Kay, L. E., Wingfield, P. T., Bax, A., Gronenborn, A. M., and Clore, G. M. (1989) *Biochemistry 28*, 6150−6156.
75. Kay, L. E., Xu, G. Y., Singer, A. U., Muhandiram, D. R., and Forman-Kay, J. D. (1993) *J. Magn. Reson., Ser. B 101*, 333−337.
76. Kay, L. E., Marion, D., and Bax, A. (1989) *J. Magn. Reson. 84*, 72−84.
77. Zhang, O., Kay, L. E., Olivier, J. P., and Forman-Kay, J. D. (1994) *J. Biomol. NMR 4*, 845−858.
78. Pascal, S. M., Muhandiram, D. R., Yamazaki, T., Forman-Kay, J. D., and Kay, L. E. (1994) *J. Magn. Reson., Ser. B 103*, 197−201.
79. Grzesiek, S., and Bax, A. (1992) *J. Magn. Reson. 96*, 432−440.
80. Powers, R., Gronenborn, A. M., Clore, G. M., and Bax, A. (1991) *J. Magn. Reson. 94*, 209−213.
81. Lee, W., Revington, M. J., Arrowsmith, C., and Kay, L. E. (1994) *FEBS Lett. 350*, 87−90.
82. Kraulis, P. J. (1991) *J. Appl. Crystallogr. 24*, 946−950.

BI9809019